Materials Science and Engineering C 66 (2016) 193–198

Contents lists available at ScienceDirect

Materials Science and Engineering C

journal homepage: www.elsevier.com/locate/msec

Polymer microfilters with nanostructured surfaces for the culture of circulating cancer cells

Olga V. Makarova [a,1], Daniel L. Adams [b,*,1], Ralu Divan [c], Daniel Rosenmann [c], Peixuan Zhu [d], Shuhong Li [d], Platte Amstutz [d], Cha-Mei Tang [d]

[a] Creatv MicroTech, Inc., 2242 West Harrison St., Chicago 60612, IL, United States
[b] Creatv MicroTech, Inc., 1 Deer Park Drive, Monmouth Junction, NJ 08852, United States
[c] Center for Nanoscale Materials, Argonne National Laboratory, 9700 South Cass Ave., Argonne 60439, IL, United States
[d] Creatv MicroTech, Inc., 11609 Lake Potomac Drive, Potomac 20854, MD, United States

ARTICLE INFO

Article history:
Received 27 August 2015
Received in revised form 5 April 2016
Accepted 21 April 2016
Available online 22 April 2016

Keywords:
Tumor cell culture
Structured culture
RIE treated polymer
Nanostructure
Surface topography

ABSTRACT

There is a critical need to improve the accuracy of drug screening and testing through the development of *in vitro* culture systems that more effectively mimic the *in vivo* environment. Surface topographical features on the nanoscale level, in short nanotopography, effect the cell growth patterns, and hence affect cell function in culture. We report the preliminary results on the fabrication, and subsequent cellular growth, of nanoscale surface topography on polymer microfilters using cell lines as a precursor to circulating tumor cells (CTCs). To create various nanoscale features on the microfilter surface, we used reactive ion etching (RIE) with and without an etching mask. An anodized aluminum oxide (AAO) membrane fabricated directly on the polymer surface served as an etching mask. Polymer filters with a variety of modified surfaces were used to compare the effects on the culture of cancer cell lines in blank culture wells, with untreated microfilters or with RIE-treated microfilters. We then report the differences of cell shape, phenotype and growth patterns of bladder and glioblastoma cancer cell lines after isolation on the various types of material modifications. Our data suggest that RIE modified polymer filters can isolate model cell lines while retaining ell viability, and that the RIE filter modification allows T24 monolayering cells to proliferate as a structured cluster.

1. Introduction

Circulating tumor cells (CTCs) are cancer cells transiting the circulatory system, which have originated from a primary tumor and capable of being used as source information for cancer diagnosis and the monitoring of disease [1,2]. These CTCs may provide valuable information for personalized cancer treatment, by isolating viable patient cells and culturing them to screen for their response to drugs *ex vivo*. However, efficient isolation of CTCs from peripheral blood is challenging due to their extreme rarity (~ one cell in every 10 [9] total blood cells) and the inability to retain viable cells for culture [1–3]. Among the variety of research methods developed to isolate CTCs, microfiltration is recognized as a rapid and straightforward method of isolation of CTCs from blood [3–11]. We have previously investigated various brands of microfilters, reporting on the ideal microfilter properties for CTC isolation, and described that retention of cell viability is applicable to filtration [4–6,12]. A commercially available, lithographically made CellSieve™ microfilter has been reported to be tailored for CTC isolation [4–6,12]. High capture efficiency (>90%) is provided by the 160,000 precision pores, 7 μm in diameter, uniformly distributed within a 9 mm diameter area. The microfilter material has been described as biocompatible, non-fluorescent, optically transparent and mechanically/chemically stable. Further, the biologically applicable filter material has been described as non-toxic, medical grade material, conducive to the efficient capture of cells while retaining cell viability during isolation, demonstrated to provide excellent capture efficiency for most solid tumor cancer cell lines and in patient samples [4–6,12,13].

It is imperative that CTCs are isolated without compromising cell viability so that cells might be subsequently cultured, and used for diagnostic assays and/or in evaluating pharmacokinetics of drugs. A new approach to capture and culture viable CTC is to use microfilter with nanoscale surface features to change local topological interactions [14]. It has been demonstrated that immunofunctionalized silicon nanopillars [15] and quartz nanowires [16], as well as bare RIE-generated nanorough glass surface [17] improves cancer cell capture. Three-dimensional (3D) tumor cell culture using nanoculture plates, in which nanoscale rectangular grid patterns were printed on transparent resin, has been reported [18]. Zheng et al. [19] demonstrated that

* Corresponding author.
E-mail address: dan@creatvmicrotech.com (D.L. Adams).
[1] These authors contributed equally to this study.

http://dx.doi.org/10.1016/j.msec.2016.04.075

culture of captured CTCs on microporous parylene-C membrane is possible. However, combining CTC isolation and patterned cell culture on the same microfilter would give the advantage of reduced cell loss, minimize damage and mimic physiological *ex vivo* cell growth, while providing a simple workflow [6,19].

RIE is a straight forward cost-effective technique to modify the properties of substrate surface for biomedical research [20]. We suggest that by modifying the nano-topographies on the microfilter surface might be a simple way of affecting the phenotypic growth patterns of cultured cells. We used RIE without masking and with the AAO membrane as a mask. Usually an AAO membrane for nanofabrication is obtained by a multistep anodization process using Al foil [21,22]. The membrane is then released from the Al substrate and used either as a template or as an etching mask. The fabrication of thin AAO templates directly on Si wafers was also reported [21,22]. In this work, an AAO membrane etching mask was fabricated directly on a polymer microfilter surface. Here, we report our results on RIE assisted nanopatterning of CellSieve™ polymer microfilters for patterned cancer cell culture.

2. Experimental

CellSieve™ polymer microfilters were used in all experiments.

2.1. Fabrication

O_2 RIE without masking was performed using a RIE March CS-1701 system. The O_2 flow rates were varied from 10 sccm (standard cubic centimeter per minute at standard temperature and pressure) to 45 sccm. Plasma power was 100–300 W. Sample size was 4 in. in diameter. The contact angles of water on the microfilter surfaces were measured at 20 °C with the sessile drop method. An inductively coupled plasma reactive ion etching (ICP-RIE) System 100 system (Oxford Instruments plc, Abingdon, UK) was used for polymer etching *via* AAO membrane. The AAO membrane was prepared directly on the polymer microfilter surface through a one-step anodization process. The aluminum deposition onto the microfilter surface was performed in a Lesker PVD-250 electron-beam evaporator with a Sigma deposition controller. Aluminum films with thickness of 0.5, 1 and 2 μm were prepared using the following parameters: base pressure: 1 × 10–8 Torr, deposition rate 20 Å/s. The anodization was carried out using a Keithley 2400 power supply at the constant voltage of 40 V in 0.3 M oxalic acid. The temperature of the electrolyte was maintained at 10 °C using a jacketed beaker and a cooling system (Fisher Scientific, Isotemp 3016D Circulator). The solution was stirred vigorously using a magnetic stirrer in order to accelerate dispersion of the heat generated by the sample during anodization. The oxidation process was performed until the anodization was completed and no Al layer remained under the AAO template. The anodization time was ~60, 40 and 20 min for 2, 1 and 0.5 μm thick Al layer correspondingly. The typical area of AAO membrane was ~2 cm^2. Pores in AAO were widened by dipping in a 0.1 M phosphoric acid solution at room temperature for 40–60 min. ICP-RIE was used for both the barrier layer removal and the following polymer etching. The barrier layer was removed using Cl_2 and BCl_3 gases with chamber pressure of 7 mTorr and flow rates of 20 sccm and 10 sccm respectively. The power of ICP was maintained at 150 W with constant RF power of 100 W. Polymer etching *via* AAO membrane was done with the following parameters: O_2 flow of 50 sccm, SF_6 flow of 2 sccm, chamber pressure of 50 mTorr, RF power of 200 W, temperature of 20 °C, and etching time of 2 min. After polymer etching, the AAO mask was detached from the microfilter surface using 3 M scotch tape. The surface topography was characterized using a FEI Nova 600 scanning electron microscope (SEM). Samples were sputter-coated (EMITECH) with ~10 nm of gold for SEM imaging.

2.2. Cell culture

Tumor cell lines used in this study were purchased from ATCC (Manassas, VA). These include the U251 and U87 human glioblastoma cell lines, and the T24 human bladder cancer cell line. All cell lines were grown in their respective media containing fetal bovine serum (FBS) as recommended by ATCC. Cell lines were maintained in *T*-25 or T-75 flasks using prescribed cell culture conditions (5% CO_2, 37 °C) with media changes every 3–4 days. Cells were harvested on the same day using trypsin-EDTA and stored in their respective media. Sterile microfilters, either RIE-treated microfilters or unetched microfilters, were placed in a 12-well plate with media. An empty well was used as a control for cell growth, also with media. Approximately 1000 cells were placed on each filter, or in an empty well, and were incubated in a humidified incubator at 5% CO_2 and 37 °C for 3–7 days.

For calculating the proliferation of T24 cells on RIE treated filters, untreated filters and culture wells, the following experiments were performed. Media was placed into all wells on a 12 well plate, 3 RIE filters and 3 untreated filters were placed into individual wells. Approximately 1000 T24 cells were enumerated and spiked onto the 3 RIE filters, 3 untreated filters or into 3 empty culture wells. The plate was incubated in a humidified incubator at 5% CO_2 and 37 °C for 3 days. After 3 days, all 9 wells samples were fixed, stained and imaged using a Carl Zeiss AxioCam camera (Carl Zeiss). Zen Blue analysis software (Carl Zeiss) quantified the number of DAPI cell signals in each well. The average number of cells per mm^2 after 3 days of culture were calculated in triplicate, for equal comparison.

In conjunction with direct spike in experiments, we tested the effects of the filtration process on the cell viability and phenotypic growth characteristics after filtration for the T24, U251 and U87 cell lines. Filter types, RIE or untreated, were placed into a microfilter holder (Creatv MicroTech, Inc.), approximately 1000 cells were spiked into media and filtered as previously described [4,6,23]. After filtration, microfilters were then placed in a 12-well plate with media and were incubated in a humidified incubator at 5% CO_2 and 37 °C for 3–7 days.

For determining capture efficiency and effect on cell viability during filtration, CellTracker™ Orange Cell Viability Dye was used [24]. Cancer cell lines were labeled in culture with CellTracker™ Orange (Invitrogen, cat #34551) according to manufacturer's protocols, after incubation with 5 μm CellTracker™ Orange the cells were washed to remove remaining dye. CellTracker™ Orange is an intracellular viability marker that is only retained when cells remain alive. Approximately 100 dyed cells were enumerated, added to 3 ml of normal whole blood, diluted with 3 ml PBS and filtered as previously described [5,6,12,23]. After filtration the CellTracker™ Orange was fixed within the cell, according to manufacturer's protocols, and labeled with DAPI. Filters were mounted, imaged and enumerated for capture efficiency of viable cells. Only cells positive for both CellTracker™ Orange and DAPI were considered for calculating capture efficiency, all experiments were run in duplicate (Supplementary Fig.1).

For staining cytokeratin (CK), after 3, or 7, days the filters/slides were then rinsed, fixed, and stained by an antibody cocktail of CK 8 and 18 conjugated to fluorescein isothiocyanate (FITC) dye (eBioscience, San Diego, CA) as previously described [4–6]. CK 8 is usually used together with CK 18 to differentiate cancer cells in blood [4–6]. To visualize cell nucleus, cells were stained with 4′,6-diamidino-2-phenylindole (DAPI) (Invitrogen, Carlsbad, *CA*, USA). The cells were analyzed using an Olympus BX54WI fluorescence microscope with a Carl Zeiss AxioCam camera (Carl Zeiss MicroImaging, Thornwood, NY).

SEM imaging of cells growing as monolayers and clusters was run as previously described [23]. Briefly, approximately 1000 cancer cell lines, U87 or U251, were spiked onto filters within a 12 well plate and with media. The plate was incubated in a humidified incubator at 5% CO_2 and 37 °C for 7 days. Media was removed and replaced with 2.5% solution of Glutaraldehyde for 1 h at 4 °C. Filters were washed in DI water at room temp for 30 min then serially dehydrated in 70%, 80%, 90%

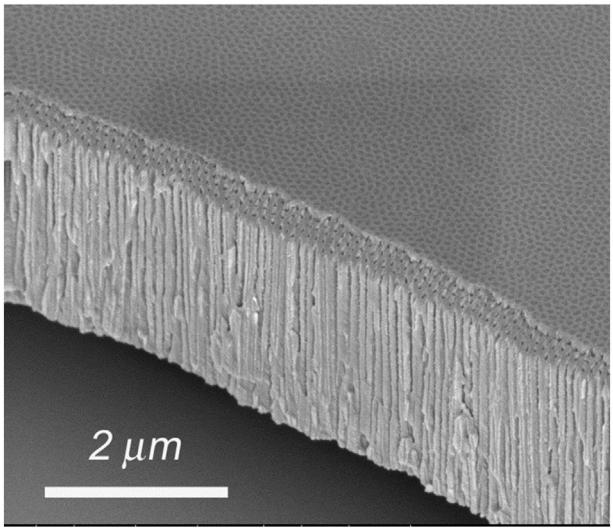

Fig. 1. A cross-sectional SEM micrograph of ~2 μm thick AAO membrane with well-ordered perpendicular to the surface pores and a barrier layer that is partially removed on the membrane edge.

and 100% ethanol for 2 min per each solution. Samples were dried, positioned onto a sample pin stub, and placed in a desiccator until imaged using a Phenom ProX Desktop Scanning Electron Microscope (NanoScience Instruments).

3. Results and discussion

3.1. AAO membrane fabrication

The conventional method for AAO template fabrication for nanofabrication is a multi-step process of anodic oxidation of aluminum foil involving the manipulation of a freestanding fragile AAO membrane [21,22]. It has been demonstrated that thin AAO templates can be fabricated directly on a Si wafer [25,26]. In order to improve long range pore ordering of the fabricated membrane, a multistep anodization process was employed. The process started with a 1.3–1.6-μm thick aluminum film, part of it is consumed by anodization and alumina dissolution until finally ~500 nm-thick well-ordered AAO membrane remained on a Si wafer. Our goal is to develop a simple, robust, one-step method, in which an AAO membrane acts as an etching mask after a single-step anodization of a thin aluminum film deposited directly on the polymer surface.

For this purpose, an aluminum film of high purity and very low roughness is required. In addition, relatively long anodization times were employed to allow for the rearranging of the AAO cells and to reduce the number of defects and dislocations [27]. Three different aluminum film thicknesses were prepared. The 2 μm aluminum film was used to evaluate the quality of the AAO fabricated on the polymer surface. Then AAO was fabricated from 1-and 0.5-μm- thick Al films and used as an etching mask for polymer surface nanopatterning. To achieve very low surface roughness, Al evaporation parameters were first optimized using Si wafer as a substrate, achieving 4.45–5.13 nm rms roughness over 1 mm area. These parameters were used for Al deposition on the polymer surface. Al anodization was conducted in 0.3 M oxalic acid at 10 °C and a constant voltage of 40 V with current density of ~3 mA/cm^2, which led to a self-ordered pore array. During the first seconds of Al oxidation, the current drops abruptly as a result of the formation of the planar oxide barrier layer. Then, the current gradually increases and after a few minutes reaches its maximum, slightly drops and remains constant through the end of the anodization process. The increase in current is characteristic for porous AAO formation, nucleating the pores, while a constant current value, indicates that the original disordered pores are becoming hexagonally ordered, implying that stationary pore growth has been attained [28]. Anodization was performed until all Al was used up and monitored by the drop in the current value and its color change to purple. To make sure no Al film remains underneath, the membrane was detached and placed up-side down for the examination. Fig. 1 shows a cross-sectional SEM micrograph of a ~2 μm-thick AAO membrane with self-aligned pores perpendicular to the surface. An hemispherical shell with homogeneous thickness of ~40 nm known as the barrier layer that developed at the bottom of every nanopore during the anodization process is seen on the membrane top. At the membrane edge, the barrier layer is partially removed and pores are visible. A very low Al roughness and a long anodization time have allowed the fabrication of straight pores for all prepared thicknesses of aluminum film.

3.2. RIE of the filters via AAO

The anisotropic etching of the polymer surface *via* the AAO etching mask was performed using ICP-RIE. AAO membranes 1 and 0.5 μm thick were used as the etching masks. To enlarge the pore diameter and to remove the barrier layer, a sample was immersed into a 5% H_3PO_4 solution for 40–60 min[29]. In some experiments, to increase the pore sizes and to fully open the barrier layer, in addition to the wet chemical etching by 5% H_3PO_4 we used Cl_2 and BCl_3 RIE [29]. An approximately 1 μm-thick AAO membrane with straight pores of 50–80 nm in diameter, and the CellSieve™ microfilter surface etched *via* this membrane by RIE for 2 min, are shown in Fig. 2a, b. The CellSieve™ microfilter surface has well-defined imprints from AAO membrane made by plasma etching through it (Fig. 2). The fact the etch pattern is not uniform, can be explained as not all pores in the AAO membrane have been fully opened for plasma to etch. The use of ~0.5 μm thick AAO mask and the same etching parameters resulted in deep polymer etching. Fig. 2c shows a cross-sectional SEM image of the ~0.5 μm thick AAO mask and the etched polymer surface created. As a comparison, an untreated microfilter has a smooth filter surface, Fig. 2d. Further optimization of the etching parameters is needed to tailor the pore size and density on the polymer surface.

3.3. Mask-less RIE of the microfilters

We also performed O_2 RIE of polymer microfilter without an etching mask. Plasma etching involves degradation of the polymer chains due to ion bombardment (physical etching and anisotropic) and chemical surface reactions due to radical reactions (chemical modification and isotropic). Both physical and chemical processes are always present during plasma treatment and never isolated from each other. Chamber pressure and beam energy are the main parameters that allow to control etching anisotropy. The lower the chamber pressure and the higher the plasma energy, the more anisotropic the resulting etching will be, displaying larger changes in the surface topography [30–32]. We varied O_2 flow rate and plasma power to achieve different surface topography. Fig. 3 shows SEM images of the surface topographies obtained at the same power of 150 W, etching time of 10 min and various O_2 flow rates. Homogeneous patterns with bumps or fibrils were observed on the microfilter surface depending on the plasma parameters similar to those observed on PET films after O_2 plasma [31]. Chemical modification of polymer microfilter by O_2 RIE changes surface properties from hydrophobic to hydrophilic. The contact angle of water on the surface decreased from about 90° to 0° after the O_2 RIE for 5 min (at an RF power of 150 W).

3.4. Cell culture

Proper growth properties while culturing cancer cells is essential for drug development and cancer research. Synthetically fabricated

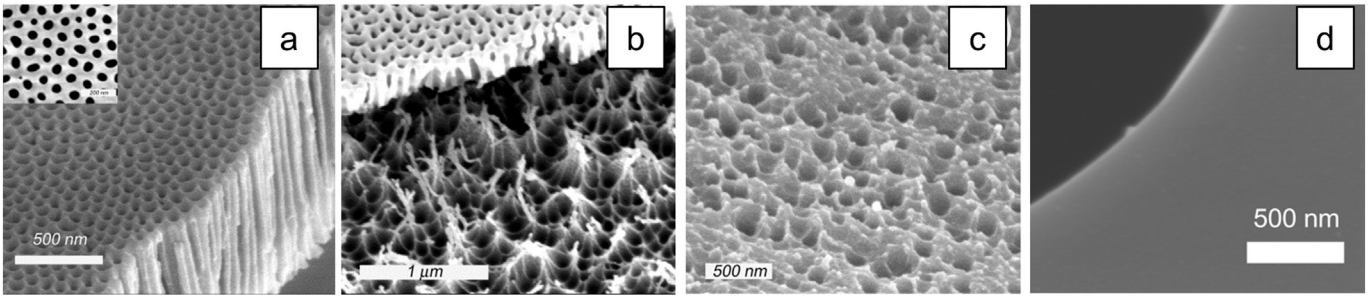

Fig. 2. SEM images of the surface topographies obtained by plasma ething *via* the AAO membranes and untreated filter surface. (a) Top (insert) and cross-sectional SEM images of the ~1 μm thick AAO membrane with pore diameters in the range of 50–80 nm; (b) a SEM image of the microfilter surface etched by O_2 RIE for 2 min *via* this AAO membrane (c) a cross-sectional SEM image of the ~0.5 μm thick AAO mask and etched microfilter surface (d) a SEM image of the untreated filter surface not altered by etching.

nanotopography such as nanometer size wires, posts, pits and gratings has been shown to influence cell morphology, alignment, adhesion, migration, and proliferation [14,30–32]. Chen et al. [17] demonstrated differential adhesion preference of cancer cells to RIE-generated nanorough glass surfaces when compared to normal blood cells. Studies were undertaken to characterize and compare the influence of polymer surface topography generated by RIE on cancer cell culture, we choose 3 cancer cell lines, known to grow as monolayers (bladder T24 and glioblastoma U251 cell line) or as structures (U87 form spheroids/domes). Cells added to filters and cultured for 3 days on the two types of polymer microfilters, or in an empty well, were examined under the inverted microscope Supplementary Fig.2. On day 0, approximately 1000 cells were used for each sample. By day 3, distinct patterns of growth were seen on the filters in all the cell lines. Cell growth patterns of T24 and U251cells in the empty culture wells appeared flat and formed the normal monolayer culture pattern [33–36]. On the untreated filters, the T24 continued to grow as the standard monolayer culture pattern (Fig. 4a, c, e) [33]. Interestingly, on the RIE treated filters, the T24 began forming clusters of domed patterns similar to the U87 cells line [35] (Fig. 4b, d, f and Fig. 5), suggesting that RIE treated filters do in fact effect the standard growth patterns of monolayering cell types. These patterns, monolayer *versus* structured growth, can further be observed by the visualization of DAPI from the T24 cells, Figs. 4c and d. The proliferation of these T24 cells was then tested and shown to be identical between standard plate culture, untreated filters and RIE treated filters suggesting that the change in the tertiary growth structure does not affect cell proliferation (Supplementary Fig. 2). With high magnification images of nuclei, one can compare the 3D growth on the RIE-modified microfilter, where nuclei can be seen on 3 separate *Z*-planes, Fig. 5a. We then applied these observations to the entire filtration process by comparing more specifically whether the monolayering phenotype of U251 glioblastoms [35] and the spheroid phenotype of U87 glioblastoma [35] were altered by the filtration of cells. After cells were filtrated and incubated for 7 days in culture, filters were removed and imaged. U251 cell growth remained as a monolayer on the filters, Fig. 5b shows a single image of the cultured cells and microfilter pores seen on the same plane. U87 cells on the microfilters grew as large domed spheroid structures, Fig. 5c, d shows cultured cells imaged on two planes, the microfilter in focus (Fig. 5c) or the cell dome in focus (Fig. 5d). The growth patterns observed suggests that both RIE treated and non-treated filters allow for distinct multidimensional structured growth of various cell lines. Further, RIE-treatment of filters can affect the growth patterns of certain monolayering cell lines, *i.e.* T24, by inducing a multidimensional growth phenotype.

To further characterize the phenotypic changes between cells grown on non-treated filters and RIE-treated filters, we stained for the intermediate filament cytokeratin. Expression of cytokeratins (CK) 8 and 18 was detected by immunofluorescence staining using anti-CK 8/18 antibodies conjugated with FITC. Nuclei were counterstained with DAPI (blue). T24 cells on untreated filters grew in 2D formats of flat monolayers expressing low-levels of diffuse CK 8/18 (Fig. 4e). However, when T24 cells were cultured on the microfilters, treated by RIE, they formed clustered islands and expressed high-levels of CK8/18, in filamentous structures (Fig. 4f). One can theorize that as cytokeratins interact with desmosomes and hemidesmosomes, collaborating to cell-cell adhesion, this may explain why there is increased cytokeratin expression in the structured forms. However, this study focused on the surface topography alteration of filters, and the observations of CK phenotype differences calls for further studies to characterize these events. While further studies are now needed to determine the distinct biological pathways altered by the two substrates, this data suggests that RIE treatment creates a surface, which has a distinct and biologically separate growth patterns than that of untreated filers.

We have shown that certain cancer cell lines can be induced into structured clusters by taking the image of the cell nuclei in different focal planes, Fig. 5a. The discrepancies in the CK8/18 expression between adherent T24 monolayering on filters and T24 cluster formation highlight the importance of the microenvironment and should be

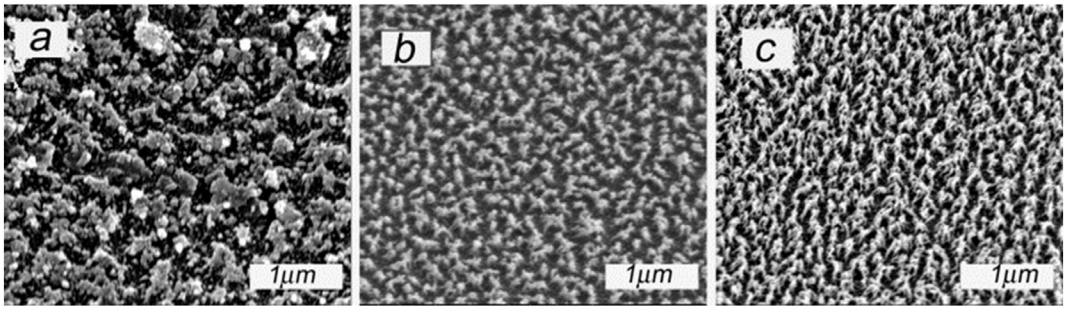

Fig. 3. SEM images of the surface topographies obtained at the same plasma power of 150 W, etching time 10 min and various O_2 flow: (a) 45 sccm (b) 20 sccm (c) 10 sccm.

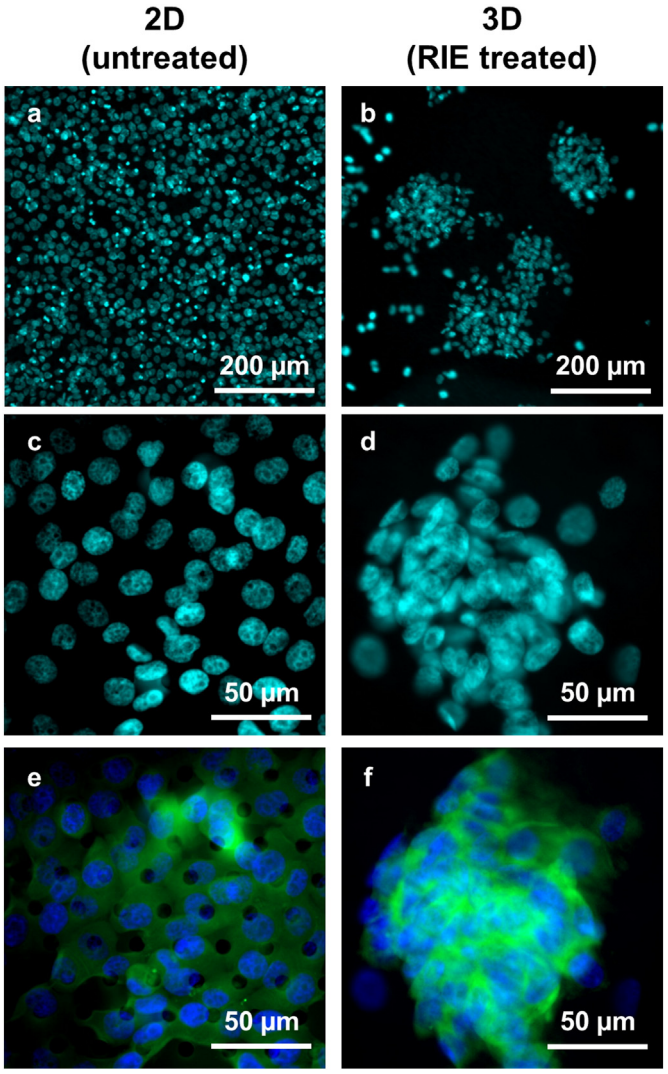

Fig. 4. Fluorescence microscope images of bladder cancer T24 cells cultured on an untreated and on a RIE-treated microfilter. (a) DAPI visualization of cultured T24 on an untreated microfilter can be seen on a single Z plane from monolayered growth. (b) DAPI visualization of T24 on a RIE treated microfilter DAPI signals are on various Z planes form clustered growth. (c) 40× magnification of the nuclei on untreated microfilter (d) 40× magnification of the nuclei on a RIE treated microfilter. (e) Expression of CK8, 18 of cells is seen by immunofluorescence staining using anti-CK8/18 antibodies conjugated with FITC (green), which appears weak and diffuse. (f) Expression of CK8, 18 of cells from the RIE treated filters, which appear intense and striated.

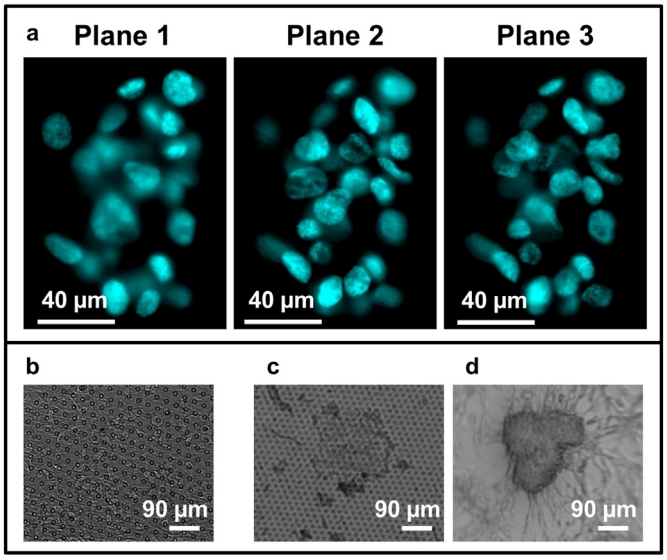

Fig. 5. Cell culture microscope images taken on the different Z focal planes for the RIE-modified surface. (a) Images of DAPI on 3 separate planes show that the T24 cell line grew as a multidimensional structure, ~3–4 cell layers high, on the RIE treated microfilter. (b) Representative U251 cell line growing on the microfilter as a monolayer on a filter. (c) Representative image of a cell line growing as a domed structure on a filter. The microfilter can be seen in focus, but the cell dome appears out of focus and hazy. (d) The top of the U87 cell line dome can be seen in focus, but as it is on a separate plane, the microfilter is now out of focus.

further investigated. These results demonstrated that surface nanotopography created by RIE can facilitate growth of cancer cells into clustering domes and thus structures more similar to tumors growing *in vivo*. Using known spheroid forming cell lines, we further demonstrated that the filtration and subsequent culture allow for the retention of known 3D tumor growth patterns and with certain nanotopographies can induce structures in otherwise monolayering cell types.

4. Summary and conclusions

We propose a simple method to alter surface properties of commercially available polymer microfilters for efficient and structured cell culture. We have demonstrated that bladder and glioblastoma cancer cell morphology and behavior are influenced by RIE-created surface nanotopography, but not the filtration process. To broaden the spectrum of nanotopographies that could be obtained on the microfilter surface, we used RIE without masking and with the AAO membrane as a mask. We have demonstrated that a thin AAO membrane with straight pores can be fabricated directly on a polymer surface. The changes in cell culture on RIE-modified surface may be attributed to the high surface area of the nanostructured polymer, increased surface hydrophobicity, and diminished cell-to-substrate physical contact. The use of the same microfilter for both CTC isolation from blood and for cell culture can reduce cell loss, minimize cell damage, and facilitate cell growth, while providing a simple and rapid workflow. Though preliminary, we must now assess the pharmacokinetic differences between monolayering and structured formation on the RIE treated filters using standard cell lines. In this study we tested and optimized the parameters required to grow commercial cell lines as monolayer or as 3D structures. We must now determine if the filter alterations described herein are applicable on patient derived CTCs, and if patient derived CTCs behave in a similar manner to cell lines. Interestingly, preliminary patient studies have shown that CTCs, from breast, prostate and colorectal patients, can be isolated using the methods described in this manuscript and that the cells remain viable for *ex vivo* studies [24]. Future studies will also include the addition of cancer patient CTCs, and co culture of stromal cells, to determine what topography is optimal for culture of cancer cells for use in screening drug applicable targets.

Financial support

This research was funded in part by Maryland TEDCO under MTTCF Phase I award. Use of the Center for Nanoscale Materials, Argonne National Laboratory was supported by the U. S. Department of Energy, Office of Science, Office of Basic Energy Sciences, under Contract No. DE-AC02-06CH11357.

Conflicts of interest

C.M. Tang and O. Makarova have patent applications pending related to the methods and materials in this work, application numbers PCT/US2011/030,966, US20100181288A1. D. PCT/US2012/066,390. D.

Adams, O. Makarova, P. Zhu, S. Li, P. Amstutz and CM. Tang are employees of Creatv Microtech.

Acknowledgments

Use of the Center for Nanoscale Materials, an Office of Science user Facility, Argonne National Laboratory was supported by the U. S. Department of Energy, Office of Science, Office of Basic Energy Sciences, under Contract No. DE-AC02-06CH11357. This research was funded in part by Maryland TEDCO under MTTCF Phase I award.

Appendix A. Supplementary data

Supplementary data to this article can be found online at http://dx.doi.org/10.1016/j.msec.2016.04.075.

References

[1] M. Cristofanilli, G.T. Budd, M.J. Ellis, A. Stopeck, J. Matera, M.C. Miller, J.M. Reuben, G.V. Doyle, W.J. Allard, L.W. Terstappen, D.F. Hayes, N. Engl. J. Med. 351 (2004) 781–791.
[2] K. Pantel, R.H. Brakenhoff, B. Brandt, Nat. Rev. Cancer 8 (2008) 329–340.
[3] R.A. Harouaka, M.D. Zhou, Y.T. Yeh, W.J. Khan, A. Das, X. Liu, C.C. Christ, D.T. Dicker, T.S. Baney, J.T. Kaifi, C.P. Belani, C.I. Truica, W.S. El-Deiry, J.P. Allerton, S.Y. Zheng, Clin. Chem. 60 (2014) 323–333.
[4] D.L. Adams, O. Makarova, P. Zhu, S. Li, P. Amstutz, C. Tang, Proceedings of the 102nd Annual Meeting of the American Association for Cancer Research, Cancer Res. 71 (2011) 2369.
[5] D.L. Adams, S. Stefansson, C. Haudenschild, S.S. Martin, M. Charpentier, S. Chumsri, M. Cristofanilli, C.M. Tang, R.K. Alpaugh, Cytometry A 87 (2015) 137–144.
[6] D.L. Adams, P. Zhu, O.V. Makarova, S.S. Martin, M. Charpentier, S. Chumsri, S. Li, P. Amstutz, C.M. Tang, RSC Adv. 9 (2014) 4334–4342.
[7] F.A. Coumans, G. van Dalum, M. Beck, L.W. Terstappen, PLoS One 8 (2013), e61770.
[8] L.S. Lim, M. Hu, M.C. Huang, W.C. Cheong, A.T. Gan, X.L. Looi, S.M. Leong, E.S. Koay, M.H. Li, Lab Chip 12 (2012) 4388–4396.
[9] H.K. Lin, S. Zheng, A.J. Williams, M. Balic, S. Groshen, H.I. Scher, M. Fleisher, W. Stadler, R.H. Datar, Y.C. Tai, R.J. Cote, Clin. Cancer Res. 16 (2010) 5011–5018.
[10] S.J. Tan, R.L. Lakshmi, P. Chen, W.T. Lim, L. Yobas, C.T. Lim, Biosens. Bioelectron. 26 (2010) 1701–1705.
[11] G. Vona, A. Sabile, M. Louha, V. Sitruk, S. Romana, K. Schutze, F. Capron, D. Franco, M. Pazzagli, M. Vekemans, B. Lacour, C. Brechot, P. Paterlini-Brechot, Am. J. Pathol. 156 (2000) 57–63.
[12] D.L. Adams, S.S. Martin, R.K. Alpaugh, M. Charpentier, S. Tsai, R.C. Bergan, I.M. Ogden, W. Catalona, S. Chumsri, C.M. Tang, M. Cristofanilli, Proc. Natl. Acad. Sci. U. S. A. 111 (2014) 3514–3519.
[13] F.A. Coumans, G. van Dalum, M. Beck, L.W. Terstappen, PLoS One 8 (2013), e61774.
[14] C.J. Bettinger, R. Langer, J.T. Borenstein, Angew. Chem. 48 (2009) 5406–5415.
[15] S. Wang, H. Wang, J. Jiao, K.J. Chen, G.E. Owens, K. Kamei, J. Sun, D.J. Sherman, C.P. Behrenbruch, H. Wu, H.R. Tseng, Angew. Chem. 48 (2009) 8970–8973.
[16] S.K. Lee, G.S. Kim, Y. Wu, D.J. Kim, Y. Lu, M. Kwak, L. Han, J.H. Hyung, J.K. Seol, C. Sander, A. Gonzalez, J. Li, R. Fan, Nano Lett. 12 (2012) 2697–2704.
[17] W. Chen, S. Weng, F. Zhang, S. Allen, X. Li, L. Bao, R.H. Lam, J.A. Macoska, S.D. Merajver, J. Fu, ACS Nano 7 (2013) 566–575.
[18] Y. Yoshii, A. Waki, K. Yoshida, A. Kakezuka, M. Kobayashi, H. Namiki, Y. Kuroda, Y. Kiyono, H. Yoshii, T. Furukawa, T. Asai, H. Okazawa, J.G. Gelovani, Y. Fujibayashi, Biomaterials 32 (2011) 6052–6058.
[19] S. Zheng, H.K. Lin, B. Lu, A. Williams, R. Datar, R.J. Cote, Y.C. Tai, Biomed. Microdevices 13 (2011) 203–213.
[20] E. Sardella, P. Favia, R. Gristina, M. Nardulli, R. d'Agostino, Plasma Process. Polym. 3 (2006) 456–469.
[21] J. Huang, S. Chiam, H. Tan, S. Wang, W. Chim, Chem. Mater. 22 (2010) 4111–4116.
[22] S. Yang, G. Jeon, J. Kim, J. Mater. Chem. 22 (2012) 23017–23021.
[23] D.L. Adams, R.K. Alpaugh, S.S. Martin, M. Charpentier, S. Chumsri, M. Cristofanilli, D.K. Adams, O.V. Makarova, P. Zhu, S. Li, C.-M. Tang, S. Stefansson, RSC Adv. 6 (2016) 6405–6414.
[24] S. Stefansson, D.L. Adams, W.B. Erschler, H. Le, D. Ho, BMC Cancer (2016), http://dx.doi.org/10.1186/s12885-016-2330-1. In press.
[25] V. Gianneta, A. Olziersky, A.G. Nassiopoulou, Nanoscale Res. Lett. 8 (2013) 71.
[26] S. Hwang, J. Lee, S. Jeong, P. Lee, K. Lee, Nanotechnology 16 (2005) 850.
[27] H. Masuda, K. Fukuda, Science 268 (1995) 1466–1468.
[28] F. Li, L. Zhang, R.M. Metzger, Chem. Mater. 10 (1998) 2470–2480.
[29] C.Y. Han, G.A. Willing, Z. Xiao, H.H. Wang, Langmuir: the ACS journal of surfaces and colloids, 23 (2007) 1564–1568.
[30] W.H. Kim, S.J. Park, J.Y. Son, H. Kim, Nanotechnology 19 (2008) 045302.
[31] M. Madou, CRC Press LLC, 2002 97–100.
[32] E. Wohlfart, J. Fernandez-Blazquez, E. Arzt, A. del Campo, Plasma Process. Polym. 8 (2011) 876–884.
[33] J. Bubenik, M. Baresova, V. Viklicky, J. Jakoubkova, H. Sainerova, J. Donner, International journal of cancer, Journal international du cancer 11 (1973) 765–773.
[34] P. Gazzaniga, A. Gradilone, E. de Berardinis, G.M. Busetto, C. Raimondi, O. Gandini, C. Nicolazzo, A. Petracca, B. Vincenzi, A. Farcomeni, V. Gentile, E. Cortesi, L. Frati, Annals of oncology: official journal of the European Society for Medical Oncology/ESMO, 23 (2012) 2352–2356.
[35] A. Kolchinsky, I.B. Roninson, Anticancer Res. 17 (1997) 3321–3327.
[36] H.D. Soule, J. Vazguez, A. Long, S. Albert, M. Brennan, J. Natl. Cancer Inst. 51 (1973) 1409–1416.